Illuminating gravitational wave sources with Sgr A* flares

Pau Amaro Seoane D1,2

¹ Universitat Politècnica de València, C/Vera s/n, València, 46022, Spain ² Max Planck Institute for Extraterrestrial Physics, Giessenbachstraße 1, Garching, 85748, Germany

ABSTRACT

Sagittarius A* (Sgr A*), the supermassive black hole at the center of the Milky Way, exhibits daily energetic flares characterized by non-thermal emission in the infrared and X-ray bands. While the underlying accretion flow is a Radiatively Inefficient Accretion Flow (RIAF) peaking at radio frequencies, the mechanism powering these non-thermal transients remains debated. Stellar dynamics predict a population of faint brown dwarfs orbiting Sgr A*. These objects are progenitors of Extremely Large Mass Ratio Inspirals (XMRIs), crucial sources of low-frequency gravitational waves for the future Laser Interferometer Space Antenna (LISA) mission. We investigate whether the tidal stripping of brown dwarfs provides a viable fueling mechanism for the observed flares. Here we present highresolution hydrodynamic simulations of grazing tidal interactions coupled with a parameterized nonthermal radiation model. We demonstrate that the dynamics of the tidal fallback and subsequent viscous evolution naturally reproduce the fundamental temporal characteristics of observed flares: the peak luminosity and the characteristic 1-hour duration. We show that this fueling mechanism is dynamically viable and energetically consistent, placing strong constraints on the required efficiency of the non-thermal emission process, suggesting extreme radiative inefficiency. These findings provide compelling evidence for a hidden population of brown dwarfs in the Galactic Center. Crucially, the observed high flare frequency implies tight orbits characteristic of advanced inspirals. This establishes a direct link between electromagnetic transients and active gravitational wave sources, alerting the LISA consortium years in advance to the presence of specific XMRI systems promising exceptionally high signal-to-noise ratios for precision tests of general relativity.

Keywords: Sagittarius A* (1413) — Galactic center (565) — Supermassive black holes (1663) — Brown dwarfs (185) — Gravitational wave sources (677)

1. INTRODUCTION

The supermassive black hole at the center of the Milky Way, Sagittarius A* (Sgr A*), provides an unparalleled laboratory for studying accretion physics in the strong gravity regime. Sgr A* is characterized by a Radiatively Inefficient Accretion Flow (RIAF), with emission peaking at mm/radio frequencies. However, it also exhibits daily energetic flares observed as transient increases in non-thermal emission in the near-infrared (NIR) and X-ray bands. These events offer direct probes of the dynamics and plasma properties within a few gravitational radii (R_g) of the event horizon.

Recent multi-wavelength campaigns have established a detailed phenomenology for these flares. They typically occur 1-4 times per day (K. Dodds-Eden et al.

Email: amaro@upv.es

2009; G. Witzel et al. 2018), last about one hour, with characteristic rise and decay timescales of 15 minutes, reaching X-ray luminosities of 10^{34} – 10^{36} erg/s. The emission is distinctly non-thermal, characterized by a positive spectral slope in the NIR ($\nu F_{\nu} \propto \nu^{+0.5}$) and a negative slope in the X-ray ($\nu F_{\nu} \propto \nu^{-0.5}$) (GRAV-ITY Collaboration et al. 2021; S. D. von Fellenberg et al. 2025). High-resolution interferometry has localized the emission to compact regions orbiting Sgr A* at radii of approximately 6–10 R_g (Gravity Collaboration et al. 2023). Furthermore, the flares exhibit significant linear polarization (10–30%), suggesting emission via synchrotron radiation from accelerated electrons in a strong, organized magnetic field near the black hole (Gravity Collaboration et al. 2023).

While the emission mechanism is identified as nonthermal synchrotron radiation, the mechanism triggering these events—specifically, the source of the fuel and the trigger for particle acceleration—remains debated. Proposed fueling mechanisms include the interaction with the G2 object, accretion instabilities driven by stellar winds, or large-scale magnetic activity (O. Pfuhl et al. 2015; G. Witzel et al. 2014; G. Ponti et al. 2015; D. Calderón et al. 2025; S. M. Ressler et al. 2019).

We investigate the hypothesis that these flares are fueled by the tidal stripping of material from a brown dwarf (BD) during a grazing encounter with Sgr A*. Stellar dynamics models predict a substantial population of BDs in the Galactic Center. The interaction of these objects with the supermassive black hole has implications beyond electromagnetic flares. BDs inspiraling toward Sgr A* form Extremely-Large Mass Ratio Inspirals (XMRIs), characterized by mass ratios of $\sim 10^8$. These systems are key sources of low-frequency gravitational waves detectable by the future Laser Interferometer Space Antenna (LISA) mission (P. Amaro-Seoane 2019; P. Amaro Seoane & S.-D. Zhao 2025). Modeling the electromagnetic signatures of these tidal encounters provides a means to constrain the population of these otherwise undetectable objects.

We present hydrodynamic simulations of a grazing tidal encounter between a BD and Sgr A*. We utilize Smoothed Particle Hydrodynamics (SPH) to model the stripping of the BD's envelope and the subsequent accretion of this material. This study focuses on the dynamical viability of this fueling mechanism. Due to computational limitations in resolving the small physical mass scales involved, we employ high-mass proxy simulations to capture the gas dynamics, followed by a physically motivated renormalization.

We couple the hydrodynamic results with a parameterized non-thermal radiative model in post-processing. Our models successfully reproduce the primary dynamical constraints of Sgr A* flares. We achieve the target non-thermal luminosities, generating events peaking near 10^{36} erg/s. The modeled flares exhibit durations matching the observed 1-hour timescales. These results demonstrate that the tidal stripping of brown dwarfs provides a physically viable fueling mechanism for the observed flaring activity of Sgr A*, establishing a link between the dynamics of low-mass objects in the Galactic Center and the transient accretion phenomena near the supermassive black hole.

2. METHODOLOGY

This study utilizes high-resolution hydrodynamic simulations coupled with a parameterized radiative postprocessing model. This section details the construction of the progenitor model, the simulation techniques, the physical constraints leading to the simulation strategy, and the analysis methods employed.

2.1. Brown Dwarf Model Construction

We constructed realistic initial conditions for the progenitor brown dwarf (BD) using the Modules for Experiments in Stellar Astrophysics (MESA) code (P. P. Eggleton 1983; B. Paxton et al. 2011, 2013). We modeled the progenitor as a $0.01\,M_\odot$ object evolved for a Hubble time. The resulting stabilized one-dimensional structure is characterized by a logarithmic radius $\log_{10}(R/R_\odot) = -0.9833$ and a logarithmic effective temperature $\log_{10}(T_{\rm eff}/{\rm K}) = 2.3447$. The composition is defined by mass fractions of hydrogen X=0.7597, helium Y=0.2402, and metals $Z=10^{-4}$.

The spherically symmetric profiles derived from the MESA evolution serve as the basis for the three-dimensional Smoothed Particle Hydrodynamics (SPH) model. We initialized the SPH representation by mapping the one-dimensional MESA structure onto a configuration of N=250,000 particles. We subjected the SPH model to a dynamical relaxation phase, evolving the system using equations of motion augmented with a damping term. This procedure minimizes the bulk kinetic energy K, allowing the particles to settle into hydrostatic equilibrium.

2.2. Hydrodynamic Simulations

We performed the hydrodynamic simulations of the tidal encounter using the StarSmasher SPH code (F. A. Rasio 1991; J. C. Lombardi 1998; F. A. Rasio & J. C. Lombardi 1999; J. C. Lombardi et al. 1999). The stabilized BD model is placed on specified Keplerian orbits characteristic of XMRI progenitors around Sgr A*, which is modeled as a $4.3 \times 10^6 \, M_{\odot}$ point mass sink.

StarSmasher employs variational equations of motion to evolve the system. It calculates hydrodynamic forces by determining the pressure of each particle as a function of its local properties via the equation of state. To calculate gravitational interactions, the code implements a direct N-body summation method accelerated on NVIDIA graphics processing units (GPUs). StarSmasher utilizes a cubic spline function for the smoothing kernel. To manage shocks and prevent unphysical interparticle penetration, the code employs an artificial viscosity prescription coupled with a Balsara Switch.

2.3. Tidal Interaction and Renormalization Strategy

We analyze the dynamics of the interaction and the constraints imposed by SPH resolution, which necessitates the use of high-mass proxy simulations followed by renormalization.

2.3.1. Analytical Estimates of Tidal Stripping

We first estimate the parameters of the tidal encounter for a representative orbit. We consider the $0.01\,M_\odot$ BD orbiting Sgr A* ($M_{\rm BH}=4.3\times10^6\,M_\odot$) with an illustrative periastron distance $R_p=120\,R_\odot$ and semi-major axis $a=2560\,R_\odot$. Using the derived BD radius $R_{\rm BD}\approx0.1\,R_\odot$, the tidal radius is

$$R_t \approx R_{\rm BD} \left(\frac{M_{\rm BH}}{M_{\rm BD}}\right)^{1/3} \approx 75.5 \, R_{\odot}.$$
 (1)

For such encounters, analytical models predict the fraction of stellar mass stripped. We estimate the stripped mass using the formalism of tidal energy deposition. For a penetration factor β , the energy injected into the BD structure relative to its binding energy is given by

$$\frac{\Delta E_{\text{tide}}}{E_{\text{bind}}} \approx \left(\frac{M_{\text{BH}}}{M_{\text{BD}}}\right)^2 \left(\frac{R_{\text{BD}}}{R_p}\right)^6 T(\beta). \tag{2}$$

Adopting a representative tidal coupling coefficient $T(\beta) \sim 10^{-4}$ appropriate for our scenario, we find $\Delta E_{\rm tide}/E_{\rm bind} \approx 6.3 \times 10^{-6}$. For an n=1.5 polytropic structure appropriate for a BD, this yields an estimate of the analytically expected stripped mass:

$$\Delta M_{\rm analytical} \approx 3.8 \times 10^{-6} \, M_{\odot}.$$
 (3)

2.3.2. Resolution Constraints and Proxy Simulations

We now examine the resolution constraints of our SPH simulations. The mass resolution of the simulation, defined by the mass of a single SPH particle, $m_{\rm SPH}$, is:

$$m_{\rm SPH} = \frac{M_{\rm BD}}{N} = 4.0 \times 10^{-8} \, M_{\odot}.$$
 (4)

The critical constraint arises when considering the physical mass required to power the observed flare. As determined by the optimization detailed in Section 3, the required physical accreted mass is $M_{\rm physical} \approx 1.5 \times 10^{-7} \, M_{\odot}$ (assuming a derived non-thermal radiative efficiency $\eta_{\rm NT} \approx 10^{-8}$).

Comparing this required physical mass to the resolution limit (Eq. (4)), we find that $M_{\rm physical} \approx 3.75 \cdot m_{\rm SPH}$. A direct SPH simulation normalized to the physical BD mass would represent the entire accretion event with only approximately 4 particles. This number is insufficient to resolve the fluid dynamics of the stream.

The SPH methodology is necessary to capture the complex, three-dimensional gas dynamics of the tidal interaction. However, to resolve these dynamics accurately, we execute the SPH simulation using a high-mass proxy normalization. This proxy simulation provides the temporal evolution of the accretion rate,

 $\dot{M}_{\rm simulation}(t)$, resolving the macrophysical dynamics of the interaction.

We must renormalize the simulation output in postprocessing. We introduce a dimensionless rescaling factor, $E_{\rm strip}$, to scale down the mass accretion rate from the simulation scale to the physical scale:

$$\dot{M}_{\rm physical}(t) = E_{\rm strip} \cdot \dot{M}_{\rm simulation}(t).$$
 (5)

The SPH simulation provides the dynamical framework, while $E_{\rm strip}$ adjusts the normalization to match the physical mass scale constrained by the observations and the required radiative efficiency.

2.4. Synthetic Light Curve Generation

We generate synthetic light curves using a hybrid model that decouples the macroscopic fuel delivery (hydrodynamics) from the microscopic radiation processes (plasma physics). This study focuses on the dynamical viability of the fueling mechanism and does not explicitly model the complex plasma kinetics (e.g., magnetic reconnection or turbulence) required to accelerate electrons or generate the observed non-thermal spectrum.

The SPH simulations provide the mass accretion rate profile, $\dot{M}_{\rm sim}(t)$. After applying the rescaling factor $E_{\rm strip}$ to obtain $\dot{M}_{\rm phys}(t)$, we calculate the non-thermal luminosity $L_{\rm NT}(t)$ in the observed NIR/X-ray bands as:

$$L_{\rm NT}(t) = \eta_{\rm NT} \, \dot{M}_{\rm phys}(t) \, c^2. \tag{6}$$

The non-thermal radiative efficiency $\eta_{\rm NT}$ serves as a phenomenological parameter encapsulating the efficiency of converting accreted mass-energy specifically into the observed non-thermal radiation. This must be distinguished from the bolometric radiative efficiency of the underlying RIAF. We interpret $\eta_{\rm NT}$ as a derived physical requirement on the efficiency of the unmodeled non-thermal processes.

To model the accretion flow dynamics, we convolve $L_{\rm NT}(t)$ with a viscous disk kernel characterized by a timescale t_{ν} , producing a smooth luminosity envelope representing the bulk dynamics.

The SPH simulations do not resolve the microscopic turbulence responsible for the observed stochastic variability. Therefore, to generate realistic light curves for temporal analysis, we impose a variability structure consistent with observations. We modulate the envelope with a signal generated based on the theory of spectral estimation of J. Timmer & M. König (1995), characterized by an input Power Spectral Density (PSD) slope of -2 (consistent with observations) and 30% RMS variability.

The radiative model is defined by three primary parameters: E_{strip} , η_{NT} , and t_{ν} . We systematically ex-

plore this parameter space, optimizing the parameters by comparing the synthetic light curves against key observational constraints: Non-thermal luminosity $(10^{34} - 10^{36} \, \mathrm{erg/s})$ and duration (FWHM $\approx 0.5 - 2.0 \, \mathrm{h}$).

2.5. Temporal and Spectral Analysis Techniques

We characterize the temporal profile of the resulting light curve, $L_{\rm NT}(t)$, using standard metrics. The primary measure of duration is the Full Width at Half Maximum (FWHM). We determine the FWHM by identifying the peak luminosity, $L_{\rm peak} = {\rm max}(L_{\rm NT}(t))$, defining the half-maximum level, $L_{\rm HM} = L_{\rm peak}/2$. The FWHM duration is the time interval during which $L_{\rm NT}(t) > L_{\rm HM}$. We identify the start time $t_{\rm start}$ and end time $t_{\rm end}$ by locating the crossings of the light curve with the $L_{\rm HM}$ level. The FWHM duration is then

$$\Delta t_{\rm FWHM} = t_{\rm end} - t_{\rm start}.$$
 (7)

To characterize the asymmetry of the flare profile, we calculate the rise time (the interval required for the luminosity to increase from 10% to 90% of $L_{\rm peak}$) and the fall time (the interval for the decrease from 90% to 10% of $L_{\rm peak}$).

We analyze the variability of the light curve in the frequency domain by calculating the Power Spectral Density (PSD), P(f). This analysis verifies the characteristics of the stochastic variability imposed on the model. We estimate the PSD using Welch's method (P. D. Welch 1967). We characterize the PSD by a power-law relationship, $P(f) \propto f^{\alpha}$, determining the index α by linear regression in logarithmic space, fitting $\log_{10}(P(f))$ against $\log_{10}(f)$. We compare the derived slope α to the input slope (-2) used in the light curve generation.

3. RESULTS

We present the results of the hydrodynamic simulations and the optimized synthetic light curves for the representative orbit $(R_p=120\,R_\odot,\,a=2560\,R_\odot)$.

$3.1.\ Hydrodynamic\ Evolution$

Figure 1 illustrates the dynamics of the interaction near the periapsis passage. The visualization shows the logarithmic column density of the SPH particles. The strong tidal field of Sgr A* stretches and deforms the brown dwarf structure. Material from the outer envelope is stripped away, forming tidal tails. This stripped material subsequently falls back toward the black hole, providing the $\dot{M}_{\rm simulation}(t)$ used in the light curve modeling.

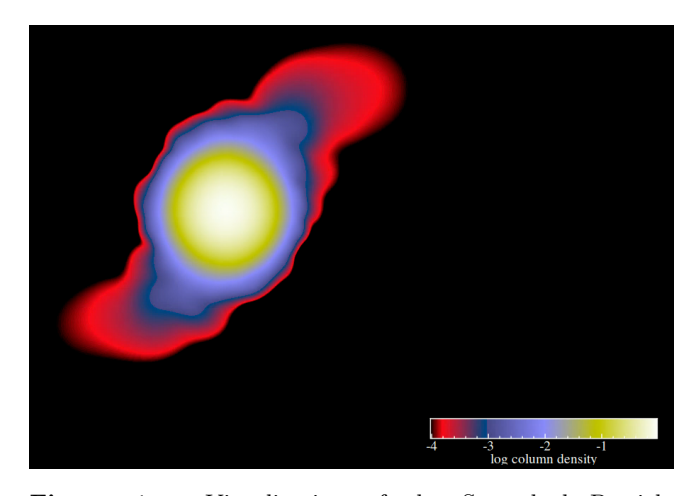


Figure 1. Visualization of the Smoothed Particle Hydrodynamics (SPH) simulation near periapsis passage $(R_p = 120\,R_\odot)$. The colour scheme represents the logarithmic column density of the gas in code units. The tidal forces exerted by Sgr A* (located off-frame) significantly stretch and deform the $0.01\,M_\odot$ brown dwarf structure. Material is stripped from the outer layers, forming the tidal streams that will subsequently fuel the accretion event.

3.2. Optimized Light Curve

The optimization of the parameter space $(E_{\rm strip}, \eta_{\rm NT}, t_{\nu})$ yielded a best fit characterized by $E_{\rm strip} = 10^{-9}, \eta_{\rm NT} = 10^{-8},$ and $t_{\nu} = 90$ minutes.

This implies a physical accreted mass $M_{\rm phys} \approx 1.5 \times 10^{-7} \, M_{\odot}$. This value is physically consistent with the mass expected from a grazing tidal encounter, although it is somewhat larger than the simple analytical estimate derived in Eq. (3). This discrepancy highlights the limitations of idealized analytical models and the necessity of hydrodynamic simulations for capturing the detailed mass loss. The derived mass confirms the necessity of the high-mass proxy approach discussed in Section 2.3.

Figure 2 displays the resulting synthetic light curve. The model successfully reproduces the key temporal features of observed Sgr A* flares. The peak luminosity reaches 8.1×10^{35} erg/s, falling within the target observational range (10^{34} – 10^{36} erg/s).

The duration of the event (FWHM) is 1.03 hours, consistent with the typical 1-hour duration observed. The characteristic rise and fall times (15.5 min and 23.3 min, respectively) also align well with observations, demonstrating that the underlying dynamics of the tidal fall-back and viscous evolution naturally reproduce the observed timescales.

4. DISCUSSION AND CONCLUSIONS

The computational models presented here establish that grazing tidal encounters between brown dwarfs (BDs) and Sgr A* provide a viable physical fueling

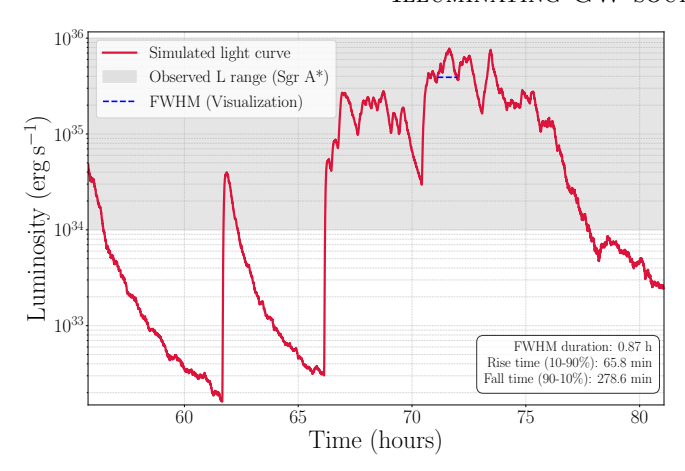


Figure 2. Temporal profile of the optimized simulation light curve. We plot the non-thermal luminosity (erg/s) against time (hours) on a semi-logarithmic scale. The solid line represents the simulated light curve, generated by imposing stochastic variability on the hydrodynamic envelope using optimized parameters: non-thermal radiative efficiency $\eta_{\rm NT}=10^{-8}$, rescaling factor $E_{\rm strip}=10^{-9}$, and viscous timescale $t_{\nu}=90$ minutes. The shaded area indicates the target observational luminosity range (10^{34} to 10^{36} erg/s). A horizontal marker illustrates the Full Width at Half Maximum (FWHM). The inset summarizes the key temporal metrics: FWHM duration (1.03 h), rise time (15.5 min), and fall time (23.3 min).

mechanism for the observed non-thermal flaring activity. Our simulations successfully reproduced the fundamental dynamical constraints derived from multiwavelength campaigns: the peak non-thermal flare luminosity (reaching $\approx 8.1 \times 10^{35}\,\mathrm{erg/s}$) and the characteristic duration ($\approx 1\,\mathrm{hour}$).

4.1. Dynamical Viability and Radiative Efficiency

The success of the model relies on the hydrodynamic processes (tidal fallback and viscous evolution) naturally reproducing the observed timescales. The flare duration is set by the viscous timescale of the compact accretion disk formed by the debris ($t_{\nu}=90$ minutes), which dominates over the shorter fuel delivery (fallback) timescale. The fact that the required viscous timescale is physically plausible for a compact, transient disk near Sgr A* supports the dynamical consistency of the scenario.

Our optimization yielded a required non-thermal radiative efficiency $\eta_{\rm NT} \approx 10^{-8}$ and a physical accreted mass $M_{\rm phys} \approx 1.5 \times 10^{-7}\,M_{\odot}$. This mass is physically plausible for a grazing tidal encounter. The derived efficiency places a stringent constraint on the underlying physics, implying extreme radiative inefficiency for the transient event.

This low efficiency is crucial for consistency with multi-wavelength observations. In standard Radiatively Inefficient Accretion Flow (RIAF) models, the thermal emission (peaking in radio/mm bands) typically dominates the non-thermal emission. While the precise partitioning of energy into non-thermal electrons is uncertain (F. Yuan et al. 2003), assuming a standard scenario where $\eta_{\rm thermal} \gg \eta_{\rm NT}$ (e.g., $\eta_{\rm NT}$ being 1-2% of the total radiated power) would imply a thermal luminosity $L_{\rm thermal} \approx 10^{38}$ erg/s. Such high radio luminosities are inconsistent with observations, which show that the NIR flare luminosity is comparable to the millimeter luminosity ($L_{\rm NIRflare} \sim L_{\rm mm}$) (GRAVITY Collaboration et al. 2020).

Therefore, the transient event must be characterized by extreme overall inefficiency, where the vast majority of the energy is advected across the horizon or lost in localized outflows, rather than radiated thermally or non-thermally. A plausible physical scenario consistent with this constraint is a two-temperature RIAF where the accretion timescale is shorter than the ion-electron energy coupling timescale. In this case, the gravitational energy, primarily stored in the ions, is advected away before it can be transferred to the electrons and radiated thermally. Detailed plasma simulations are required to confirm this hypothesis.

4.2. Sustained Flaring and the XMRI Connection

The validation of the tidal fueling mechanism establishes a robust dynamical framework, allowing us to move beyond modeling individual events toward characterizing the entire population. We analyze the potential for sustained, repeated flaring activity, as observed by monitoring campaigns (K. Dodds-Eden et al. 2009; G. Witzel et al. 2018). Given the required mass per flare $(\Delta M \approx 1.5 \times 10^{-7} \, M_{\odot})$, a $0.01 \, M_{\odot}$ BD can sustain approximately 67,000 flares.

To observe the activity as distinct flares, the orbital period T must exceed the flare duration ($\Delta t_{\rm flare} \approx t_{\nu} = 1.5$ hours). Adopting a conservative lower limit for clear separation, $T_{\rm min} \approx 4\,t_{\nu} = 6$ hours, defines the maximum sustainable flare frequency: 4 events per day. This theoretical maximum aligns with the observed daily flare rates.

This maximum frequency corresponds to a tight orbit $(a \approx 271\,R_{\odot})$ with a periastron near the tidal radius $(R_p \approx 75.5\,R_{\odot})$, or $8.3\,R_g$, consistent with astrometric localization of flares (Gravity Collaboration et al. 2023). This configuration characterizes an XMRI in an advanced stage of inspiral. The lifetime of the BD in this representative configuration is approximately 46 years.

4.3. Implications for Multi-messenger Astronomy

The ability to identify active XMRI systems via their electromagnetic flares represents a paradigm shift in

multi-messenger astronomy. It establishes an early warning system, alerting the LISA consortium years in advance to specific, localized sources. These sources are predicted to generate exceptionally high signal-to-noise ratios (SNRs) (P. Amaro-Seoane 2019; P. Amaro Seoane & S.-D. Zhao 2025), potentially eclipsing even those of supermassive black hole mergers. This foresight is critical, providing the necessary lead time to develop the specialized data analysis pipelines required to extract these complex, dominant signals.

The scientific reward is profound: these 'golden binaries' will enable measurements of Sgr A*'s fundamental parameters with breathtaking precision—constraining its spin to one part in 10¹⁰ and its mass to within a few solar masses (V. Vázquez-Aceves et al. 2023, 2025). This unprecedented accuracy transforms Sgr A* into a precision laboratory for strong-field gravity, facilitat-

ing definitive tests of the Kerr metric. While enhanced GRAVITY observations can corroborate these predictions, LISA will provide the smoking-gun evidence for this EM-GW synergy.

ACKNOWLEDGMENTS

PAS is indebted with Salvador Ardid for the access to the computational resources which allowed to do the simulations, to James Lombardi for his guidance with the SPH code and to Sebastiano von Fellenberg for discussions.

Software: MESA (B. Paxton et al. 2011, 2013; P. P. Eggleton 1983), StarSmasher (F. A. Rasio 1991; J. C. Lombardi 1998; F. A. Rasio & J. C. Lombardi 1999; J. C. Lombardi et al. 1999)

REFERENCES

Amaro-Seoane, P. 2019, Phys. Rev. D, 99, 123025, doi: 10.1103/PhysRevD.99.123025

Amaro Seoane, P., & Zhao, S.-D. 2025, arXiv e-prints, arXiv:2504.20147, doi: 10.48550/arXiv.2504.20147

Calderón, D., Cuadra, J., Russell, C. M. P., et al. 2025, Astron. Astrophys., 693, A180,

doi: 10.1051/0004-6361/202452800

Dodds-Eden, K., Porquet, D., Trap, G., et al. 2009,Astrophys. J., 698, 676,doi: 10.1088/0004-637X/698/1/676

Eggleton, P. P. 1983, Astrophys. J., 268, 368, doi: 10.1086/160960

GRAVITY Collaboration, Abuter, R., Amorim, A., et al. 2020, Astron. Astrophys., 638, A2, doi: 10.1051/0004-6361/202037717

GRAVITY Collaboration, Abuter, R., Amorim, A., et al. 2021, Astron. Astrophys., 654, A22, doi: 10.1051/0004-6361/202140981

Gravity Collaboration, Abuter, R., Aimar, N., et al. 2023, Astron. Astrophys., 677, L10, doi: 10.1051/0004-6361/202347416

Lombardi, J. C. 1998, PhD thesis, Cornell University, New York

Lombardi, J. C., Sills, A., Rasio, F. A., & Shapiro, S. L. 1999, Journal of Computational Physics, 152, 687, doi: 10.1006/jcph.1999.6256

Paxton, B., Bildsten, L., Dotter, A., et al. 2011, Astrophys.
J., Suppl. Ser., 192, 3, doi: 10.1088/0067-0049/192/1/3

Paxton, B., Cantiello, M., Arras, P., et al. 2013, Astrophys. J., Suppl. Ser., 208, 4, doi: 10.1088/0067-0049/208/1/4

Pfuhl, O., Gillessen, S., Eisenhauer, F., et al. 2015, Astrophys. J., 798, 111,

doi: 10.1088/0004-637X/798/2/111

Ponti, G., De Marco, B., Morris, M. R., et al. 2015, Mon. Not. R. Astron. Soc. , 454, 1525, doi: 10.1093/mnras/stv1537

Rasio, F. A. 1991, PhD thesis, Cornell University, New York
Rasio, F. A., & Lombardi, Jr., J. C. 1999, Journal of
Computational and Applied Mathematics, 109, 213,
doi: 10.48550/arXiv.astro-ph/9805089

Ressler, S. M., Quataert, E., & Stone, J. M. 2019, Mon. Not. R. Astron. Soc. , 482, L123, doi: 10.1093/mnrasl/sly201

Timmer, J., & König, M. 1995, Astron. Astrophys., 300, 707
Vázquez-Aceves, V., Lin, Y., & Torres-Orjuela, A. 2023,
Astrophys. J., 952, 139, doi: 10.3847/1538-4357/acde51

Vázquez-Aceves, V., Lin, Y., & Torres-Orjuela, A. 2025, Astrophys. J., 987, 208, doi: 10.3847/1538-4357/ade149

von Fellenberg, S. D., Roychowdhury, T., Michail, J. M., et al. 2025, Astrophys. J. Lett., 979, L20, doi: 10.3847/2041-8213/ada3d2

Welch, P. D. 1967, IEEE Transactions on AgriFood Electronics, 15, 70

Witzel, G., Ghez, A. M., Morris, M. R., et al. 2014, Astrophys. J. Lett., 796, L8, doi: 10.1088/2041-8205/796/1/L8

Witzel, G., Martinez, G., Hora, J., et al. 2018, Astrophys. J., 863, 15, doi: 10.3847/1538-4357/aace62

Yuan, F., Quataert, E., & Narayan, R. 2003, Astrophys. J., 598, 301, doi: 10.1086/378716